# Enhancing Quantum Yield via Local Symmetry Distortion in Lanthanide-Based Upconverting Nanoparticles

Michael D. Wisser,*,[†] Stefan Fischer,[‡] Peter C. Maurer,[§] Noah D. Bronstein,[‡] Steven Chu,[§,⊥] A. Paul Alivisatos,[‡] Alberto Salleo,*,[†] and Jennifer A. Dionne*,[†]

[†]Department of Materials Science and Engineering, [§]Department of Physics, and [⊥]Department of Molecular and Cellular Physiology, Stanford University, Stanford, California 94305, United States

[‡]Materials Sciences Division, Lawrence Berkeley National Laboratory, Berkeley, California 94720, United States

**S** *Supporting Information*

**ABSTRACT:** Lanthanide-based upconverting nanoparticles exhibit significant promise for solar energy generation, biological imaging, and security technologies but have not seen widespread adoption due to the prohibitively low efficiencies of current materials. Weak transition dipole moments between 4f orbitals hinder both photon absorption and emission. Here, we introduce a novel way to increase the radiative transition rates in Yb,Er-based upconverting nanoparticles based on local symmetry distortion. Beginning from a host matrix of the well-studied hexagonal ($\beta$)-phase $NaYF_4$, we incrementally remove $Y^{3+}$ ions and cosubstitute



for them a 1:1 mixture of $Gd^{3+}$ and $Lu^{3+}$. These two ions act to expand and contract the lattice, respectively, inducing local-level distortion while maintaining the average host structure. We synthesize a range of $\beta$-$NaY_{0.8-2x}Gd_xLu_xF_4$:$Yb_{0.18}Er_{0.02}$ nanoparticles and experimentally confirm that particle size, phase, global structure, and $Yb^{3+}$ and $Er^{3+}$ concentrations remain constant as $x$ is varied. Upconversion quantum yield is probed as the degree of cosubstitution is varied from $x = 0$ to $x = 0.24$. We achieve a maximum quantum yield value of 0.074% under 63 $W/cm^2$ of excitation power density, representing a 1.6× enhancement over the unmodified particles and the highest measured value for near-infrared-to-visible upconversion in sub-25 nm unshelled nanoparticles. We also investigate upconversion emission at the single-particle level and report record improvements in emission intensity for sub-50 nm particles. Radiative rate enhancements are confirmed by measuring excited-state lifetimes. The approach described herein can be used in combination with more established methods of efficiency improvement, such as adding passivating shells or coupling to plasmonic nanoantenas, to further boost the upconversion quantum yield.

**KEYWORDS:** upconversion, lanthanides, quantum yield, radiative rate, optical selection rules, crystal symmetry
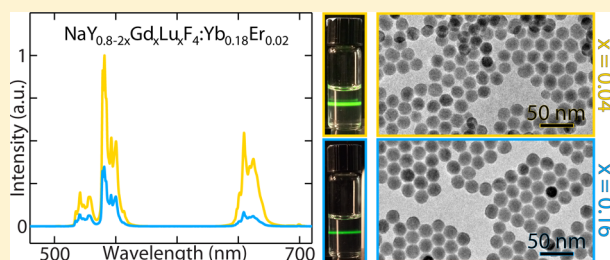
Photon upconversion (UC) describes the creation of a high-energy photon from two or more lower energy photons. Recent advances in syntheses,[1−5] materials,[6−13] and implementation techniques[14−16] have contributed to a resurgence of enthusiasm surrounding UC. Much of the innovation in the field has been driven by researchers seeking to boost the efficiency of solar cells[6,17−27] or searching for a biocompatible and background-free fluorescence imaging technology.[28−36] For these applications as well as security, display, and photo-detection technologies,[37−42] lanthanide-doped nanoparticles constitute an attractive class of materials. These materials generally absorb near-infrared (NIR) light and subsequently convert it to visible light. This NIR-to-visible type of UC is ideal for relatively wide band gap photovoltaic technologies which are not conveniently converted into tandem architectures.[17,19] Moreover, NIR light generally penetrates more deeply through and is less damaging to biological tissue compared to other photon energies.[30,32,36,39] The ability to utilize NIR excitation coupled with an inherently high signal-to-noise ratio (due to the fact that no component of tissue

naturally upconverts) makes lanthanide-based upconverters an attractive candidate for bioimaging applications.

Current lanthanide-based upconverting nanoparticles, however, remain hindered by low quantum efficiencies: 100 nm particles of the longtime standard material, hexagonal- or $\beta$-phase $NaYF_4$ codoped with $Yb^{3+}$ and $Er^{3+}$, have demonstrated a UC quantum yield of 0.3% (considering only the green emission bands of $Er^{3+}$) when illuminated with 150 $W/cm^2$ of 980 nm light.[43] For 10 nm particles of the same composition under the same incident power, this value drops to 0.005% as a result of the increased impact of surface quenching.[26,43,44] Reasons that contribute to these low efficiencies are weak absorption in $Yb^{3+}$ and prevalent nonradiative relaxation of excited $Er^{3+}$ states via coupling to host lattice phonon modes.[7,14,15,30,45−48] Both of these deleterious effects stem from the parity-forbidden nature of every transition involved in

lanthanide-based materials systems. Concisely, the parity selection rule states that electric dipole transitions that do not include a change in parity cannot occur.[49] This rule hinges on the assumption that the initial and final states involved in the transition exhibit definite parity (i.e., belong to a centrosymmetric point group). As a result, the selection rule can be circumvented by distorting the symmetries of the states in question such that they have neither definitely even nor definitely odd parity. Achieving parity selection rule relaxation in the $\beta$-NaYF$_4$:Yb,Er UC system would engender more probable absorption and radiative emission events and therefore yield an overall enhancement to quantum yield.

Our previous research in this direction has achieved successful emission enhancement using mechanical compression to distort the host matrix.[47] Notably, hydrostatic pressure was used to enhance the overlap between the host lattice ion atomic orbitals and those of the dopant lanthanides. This increased overlap led to enhanced orbital mixing and, given the pressure-distorted symmetry of the host, reduced selection rule applicability. The external stresses required to accomplish this modulation, however, are on the order of several hundred MPa. The observed UC emission increase is correspondingly limited by the plastic deformation and crystal damage that occur under such harsh conditions. Inducing lattice modulation in the absence of external means and without simultaneously damaging the host matrix thus remains an open pathway toward improved efficiencies in lanthanide-based upconverting nanoparticles.

Here, we demonstrate an enhancement in UC quantum yield via direct manipulation of the local symmetry environments of the dopant ions in $\beta$-NaYF$_4$:Yb,Er nanoparticles. We achieve this improvement by cosubstituting (i.e., substituting in equal parts) Gd$^{3+}$ and Lu$^{3+}$ for Y$^{3+}$ in the host lattice. The slightly larger Gd$^{3+}$ and slightly smaller Lu$^{3+}$[50] compensate one another such that as Y$^{3+}$ is systematically replaced, the average, large-scale structure of the host remains unchanged, but the nearest neighbor environment of any given Yb$^{3+}$ or Er$^{3+}$ ion becomes distorted. In this fashion, we are able to increase transition dipole moments without deleteriously affecting the global lattice. By simultaneously monitoring UC quantum yield and excited-state lifetimes as a function of the degree of cosubstitution, we are able to probe beneficial changes to the radiative rates of the system. We further characterize the morphology, structure, and composition of our nanoparticles using transmission electron microscopy (TEM), X-ray diffraction (XRD), and inductively coupled plasma optical emission spectrometry (ICP-OES), respectively. Using these techniques we confirm that cosubstitution yields particles that are unchanged by all metrics other than local symmetry. Together our experiments highlight the importance of host lattice symmetry and provide a facile, reliable, and broadly implementable framework for substantially improving the quantum yield of any lanthanide-based upconverting system.

$\beta$-Phase nanoparticles of composition NaY$_{0.8-2x}$Gd$_x$Lu$_x$F$_4$:Yb$_{0.18}$Er$_{0.02}$ were colloidally synthesized following a procedure described by Wang et al.[1] Samples were made spanning the range $x = 0$ to $x = 0.24$ in increments of 0.04, where $x$ is hereafter termed the "cosubstitution value". The structure of $\beta$-NaYF$_4$ is shown in Figure 1a. The vertices of the unit cell are occupied by Y$^{3+}$ ions, while the internal cation sites are occupied by a random, 1:1 mixture of Y$^{3+}$ and Na$^+$ ions. It has been shown previously that this cation disorder produces a distribution of cation-F$^-$ bond lengths throughout
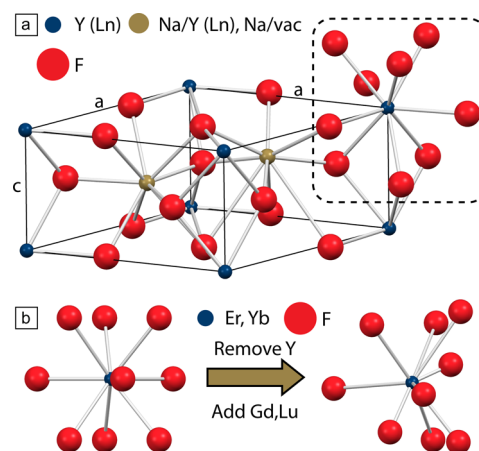


**Figure 1.** Host lattice structure. (a) Schematic depicting the unit cell of $\beta$-NaYF$_4$; basal edges are of length $a$ and the cell height is given by $c$. One internal site is occupied by Na$^+$ and Y$^{3+}$ (1:1), while the second contains a Na$^+$ ion. Y$^{3+}$ and F$^-$ ions are located at the cell vertices (blue) and interstices (red), respectively. Dopant lanthanides introduced are assumed to occupy the Y$^{3+}$ sites as shown. (b) Diagrams considering only the nearest neighbor environment of a given absorbing or emitting lanthanide ion (i.e., Yb$^{3+}$ or Er$^{3+}$, respectively), such as the boxed region in (a). In the native, unmodified material (left), the upconverting ions experience a trigonal tricapped prismatic crystal environment. When the cosubstitution value is nonzero (right), we hypothesize that the F$^-$ positions will be altered such that the symmetry of the site becomes distorted. Note that the resultant distortion is exaggerated for clarity and that the Gd$^{3+}$ and Lu$^{3+}$ ions (not shown) randomly occupy Y$^{3+}$ sites in the second-nearest-neighbor shell of the Yb$^{3+}$/Er$^{3+}$ in question.

the host.[46,51] Specifically, due to the differences in size and valency between the two cations, bonds between Y$^{3+}$ and F$^-$ will be shorter than the average cation−F$^-$ bond length in the lattice, while Na$^+$−F$^-$ bonds will be longer than the average. As a result, the local environments experienced by the Yb$^{3+}$ and Er$^{3+}$ ions (which reside in the Y$^{3+}$ sites in the host matrix) are slightly distorted from perfect trigonal tricapped prismatic symmetry. This symmetry reduction has been touted as one of the primary reasons, alongside favorable phonon mode energies, that $\beta$-NaYF$_4$ typically yields very high efficiencies as a host material for lanthanide-based UC.[7,46,51]

We hypothesized that we could achieve even higher UC quantum yields by exacerbating this local symmetry reduction. Namely, by cosubstituting Gd$^{3+}$ (which has an ionic radius of 107.8 pm) and Lu$^{3+}$ (100.1 pm) for Y$^{3+}$ (104.1 pm),[50] we sought to further expand the cation−F$^-$ bond length parameter space. Our rationale is depicted graphically in Figure 1b. In the unperturbed material, each of the F$^-$ anions that coordinates a given dopant Yb$^{3+}$ or Er$^{3+}$ ion is also bonded to some combination of Y$^{3+}$ and Na$^+$ cations. When Gd$^{3+}$ and Lu$^{3+}$ are introduced, the total number of possible bonding configurations is significantly increased. We therefore expect the magnitude of distortion to the symmetry environments of each upconverting ion to increase in a similar fashion. Our hypothesis is inspired by prior work showing improved upconversion with Li$^+$ or Mn$^{2+}$ doping.[52−56] However, employing a single dopant does not allow for independent control of both the local host matrix symmetry and the global lattice constant. Given the known sensitivity of lanthanide-based upconverting materials to the size and geometry of the host lattice unit cell,[47] such control is extremely important. We
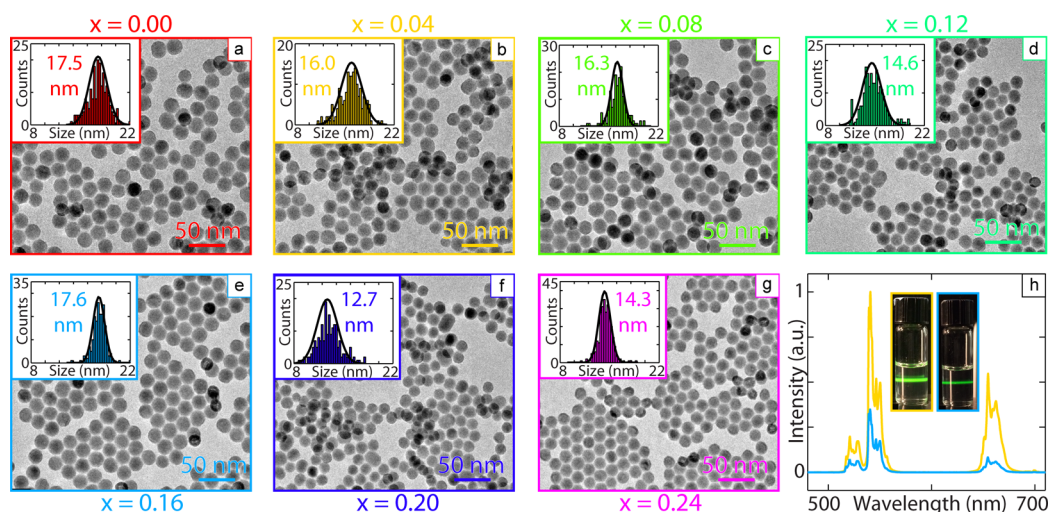
**Figure 2.** Nanoparticle size and uniformity. (a–g) TEM micrographs showing a representative collection of nanoparticles for each sample. Nanoparticle size histograms are included as insets for each sample; each shows the number of particles counted throughout the range of 8−22 nm in diameter. Gaussian curves are used to fit the histograms and extract the center, which is displayed. The standard deviation in each case is 2 nm or less. (h) Representative UC spectra obtained by irradiating the $x = 0.04$ (orange) and $x = 0.16$ (blue) samples with 100 mW of 980 nm light. Photographs are included (inset) to further demonstrate the impact of cosubstitution on UC emission. Both samples are suspended in cyclohexane at equal concentrations by mass.
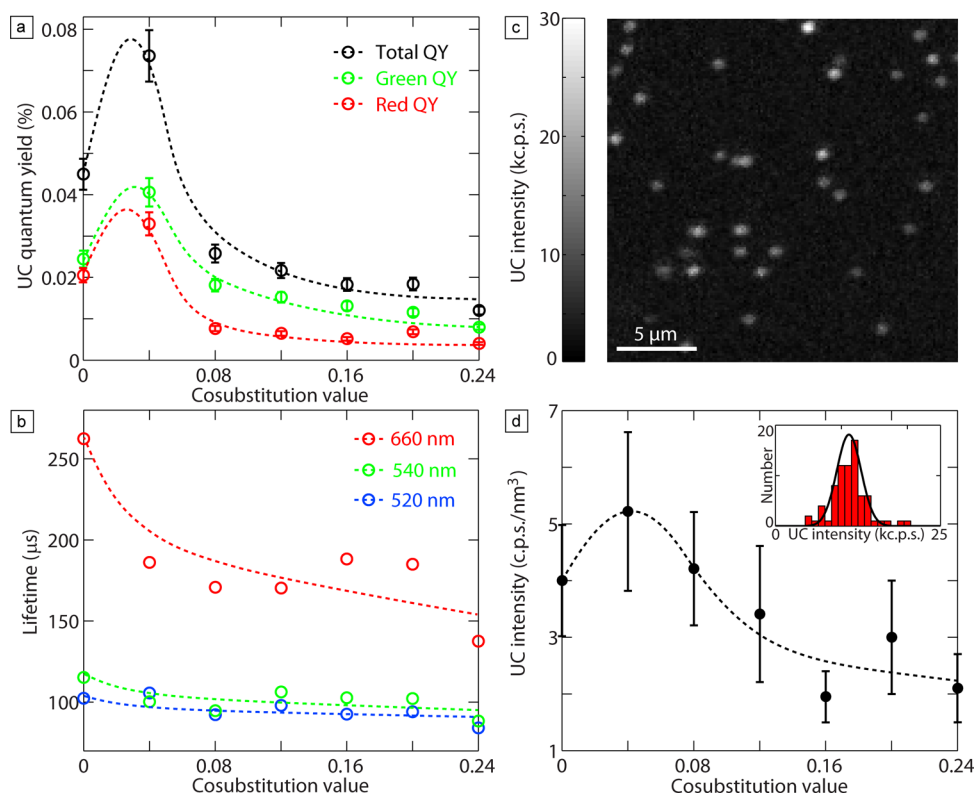


**Figure 3.** UC emission characteristics. (a) UC quantum yield as a function of cosubstitution value. The total quantum yield (black) is shown as well as that of just the green emission (green) and that of only the red (red). Guides to the eye (dotted lines) are included for each to highlight the observed trends. Error bars convey the magnitude of systematic as well as statistical uncertainty. (b) Excited-state lifetime values for the $Er^{3+}$ emission bands centered at 660 nm (red), 540 nm (green), and 525 nm (blue) obtained under 40 W/cm² of 980 nm illumination as well as guides to the eye (dotted lines) for each. Values were extracted from the lifetime traces (see SI) by determining the time required for each emission peak to reach half of its initial intensity. (c) Example optical micrograph captured under 980 nm illumination for the $x = 0.04$ sample showing emission from single particles (subsequently confirmed via SEM correlation). (d) Single-particle UC emission intensity (shown in counts per second per nm³) as a function of composition. Intensities were collected for at least 50 particles in each sample to generate histograms like the example shown in the inset. These were fit to Gaussian curves (solid line), and the center values were normalized by the particle size for each sample to obtain volumetric emission intensities.

specifically chose $Gd^{3+}$ and $Lu^{3+}$ so that the changes engendered by each would modify the local symmetry while keeping the global lattice constant of the material unchanged.

The influence of particle size (especially in regimes below 100 nm) on quantum yield in upconverting nanoparticles has been thoroughly demonstrated in recent years.[31,43,44,57] As is common in luminescent nanoparticles, the lowered efficiency with reduced particle size results from the prevalence of surface quenching in most lanthanide-based upconverters.[26,44] It is therefore crucial that the average nanoparticle diameter in each sample investigated here remains within a sufficiently narrow range such that particle size effects do not mask any efficiency changes engendered by cosubstitution. Figure 2a−g show representative micrographs for each set of nanoparticles and provide a qualitative sense of the degree of monodispersity of each sample. Particles in each sample exhibit very good size and shape uniformity, as is quantified by the histograms included as insets. Each histogram was generated using a minimum of 200 particles, and the distributions were fit to Gaussian curves, the centers of which are taken to be the particle size for each sample. A slight variation in size is apparent throughout the cosubstitution series, although the total spread is less than 5 nm in magnitude. Also note that nanoparticles in the unmodified sample (i.e., $x = 0$) are among the largest studied, so any enhancements attained via cosubstitution cannot be attributed to particle size. Finally, Figure 2h shows representative spectra as well as photographs of samples with different amounts of cosubstitution. As the plot demonstrates, varying $x$ from 0.04 to 0.16 induces more than a 3× modulation of the UC emission peak intensity. This intensity change is easily visible with the naked eye (the sample solutions are controlled for concentration by mass) and points toward the validity and promise of cosubstitution as a means for UC quantum yield enhancement.

To measure quantum yield, we excite the nanoparticles with a 980 nm diode laser and collect the resulting upconverted emission in an integrating sphere. We define UC quantum yield as the total number of visible-wavelength photons emitted divided by the number of NIR photons absorbed. Details regarding the involved measurements and data analysis can be found in the SI. Absolute quantum yield data are shown in Figure 3a. All measurements were performed using an excitation power density of 63 $W/cm^2$ at a wavelength of 980 nm. At this power, the unmodified particles exhibit a total quantum yield of 0.045%, a value consistent with previous reports in the literature.[43] Upon slight cosubstitution ($x = 0.04$), the quantum yield jumps to 0.074%, corresponding to a 1.6× enhancement. This is to our knowledge the highest ever measured NIR-to-visible UC quantum yield in unshelled nanoparticles smaller than 25 nm in size.

Figure 3a also includes quantum yield data when integrating photons from only the green-emitting transitions (i.e., the emissions centered near 525 and 540 nm) and, conversely, when considering only photons from the red-emitting transition (660 nm). After the initial enhancement engendered by a cosubstitution value of 0.04, the two quantum yield components exhibit moderately different behavior. Both quantities fall sharply when the cosubstitution value is raised from 0.04 to 0.08; as $x$ is increased beyond this point, however, the green UC quantum yield gradually declines from 0.018% to its minimum value of 0.008%, whereas the red component of the quantum yield varies only slightly from 0.008% to 0.004%. In other words, the red UC quantum yield approaches its minimum at a lower degree of cosubstitution than does the

green UC quantum yield, suggesting that the former is more sensitive to cosubstitution-induced quenching mechanisms than is the latter.

We can glean some insight from this observation by first noting that the fundamental difference between green and red emission in this materials system is the number of NIR photons necessary for each (assuming perfectly efficient UC). It is well known that radiative emission from the 525 and 540 nm peaks of $Er^{3+}$ requires two NIR photons to generate each upconverted photon.[58] Recently, however, it has been demonstrated that the $^4F_{9/2}$ state responsible for 660 nm emission is predominantly populated via a three-photon process in which the higher energy $Er^{3+}$ $^2K_{15/2}$ level is involved as an intermediate state (see SI for more details as well as a complete energy level diagram).[58] Furthermore, this manifold lies close in energy to the $^6P_{7/2}$ level of $Gd^{3+}$.[59] We propose that the increased sensitivity of the red-emitting transition to cosubstitution arises from energy transfer from the $Er^{3+}$ $^4F_{9/2}$ state to the $Gd^{3+}$ $^6P_{7/2}$ state.

While $Gd^{3+}$ energy transfer can explain the relative differences in the variations of the red and green UC quantum yield components with cosubstitution, we do not believe it is solely responsible for the general decrease observed in the overall UC quantum yield after $x = 0.04$. Purely considering local symmetry distortion, we expect cosubstitution to yield a monotonic enhancement in quantum yield. Cosubstitution may increase the prevalence of lattice imperfections, such as site vacancies and defects, which can behave as quenching centers. Given the similar ionic radii and chemical properties of $Y^{3+}$, $Gd^{3+}$, and $Lu^{3+}$, we do not anticipate substantial defect induction as the host composition is varied; however, our previous work demonstrated that UC emission in $\beta$-$NaYF_4$:Yb,Er nanoparticles is very sensitive to defect concentration.[47] Additional experiments are required to confirm the source of the quantum yield decrease beyond a cosubstitution value of 0.04.

In conjunction with quantum yield, knowledge of excited-state lifetimes is necessary to interrogate variations in the radiative rates of the system. Figure 3b shows lifetime values for each of the three radiative $Er^{3+}$ transitions as a function of cosubstitution value. The lifetimes for all transitions display an overall decrease with increasing cosubstitution. Moreover, the biggest change in lifetime occurs when $x$ is changed from 0.00 to 0.04, paralleling the quantum yield enhancement. Given the concurrent excited-state lifetime decrease and quantum yield increase, we can confirm that modifying the host lattice influences and enhances the radiative transition rates in the upconverting nanoparticles studied. That the lifetimes continue to shorten as $x$ is increased (and quantum yield drops) is indicative of nonradiative relaxation pathways becoming more favorable; this observation is consistent with the preceding hypothesis regarding the quantum yield decrease at higher values of cosubstitution. Similarly, we note that the lifetimes of the green transitions exhibit a relative decrease much smaller than that of the red transition. This discrepancy further supports the hypothesis that the $Gd^{3+}$ $^6P_{7/2}$ state siphons energy that would otherwise populate the red-emitting state in $Er^{3+}$. Despite the nuanced interplay of all of the above factors, a distinctive trend of enhanced UC quantum yield alongside reduced excited-state lifetimes for small cosubstitution values remains. We observe the same trend when exciting the $Er^{3+}$ states directly (see the SI for these data and further discussion), confirming the effects to originate from radiative rate
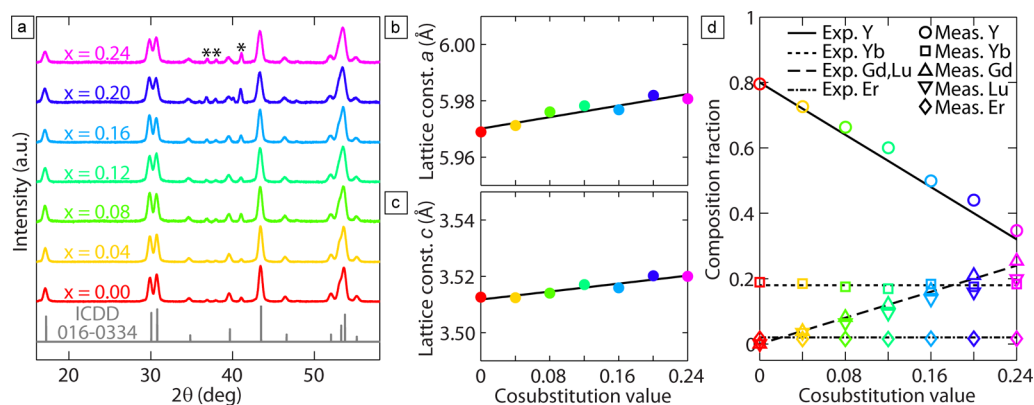
**Figure 4.** Structural and chemical characterization. (a) XRD patterns for each sample obtained using Cu K$\alpha_1$ X-rays ($\lambda$ = 1.540 56 Å). Each is consistent with the ICDD 016-0334 standard pattern (gray) with the exception of the marked peaks (asterisks); these arise from the aluminum sample holder. (b, c) Lattice constants $a$ and $c$, respectively. Values were obtained by fitting the experimental diffraction patterns to a P63/m unit cell using a recursive Pawley fitting routine. Guides to the eye are included to emphasize the slight increase in lattice constant with cosubstitution. (d) ICP-OES data obtained via dissolution of the nanoparticles in nitric acid. For each element in question, expected values (Exp.) are plotted as lines, while measured concentrations (Meas.) are shown as discrete data points.

modulation rather than changes in Yb−Er energy transfer processes.

To deconvolve the effect of particle heterogeneity in our quantum yield measurements, we also study single-particle emission intensity. Measurements are conducted using dilute samples that are deposited on glass microscope slides via spin coating. The samples are imaged in a confocal microscope and simultaneously excited using 980 nm light (see SI for more details). UC emission intensity is monitored as a function of sample position, as shown in Figure 3c. Finally, the samples are gold-sputtered and imaged using a scanning electron microscope (SEM). Fiducial markers are used to correlate the measured emission values to single particles located in SEM scans. Single-particle UC emission intensities are recorded for a minimum of 50 nanoparticles in each sample. The resultant distributions are fit to Gaussian curves to extract a representative intensity value for each sample. Finally, these values are normalized by the corresponding particle size to generate volumetric emission intensities; these data are shown in Figure 3d, as is an example histogram for the case of $x = 0$. This plot demonstrates that single-particle emission intensity follows the same trend as that observed in total UC quantum yield. Again, a cosubstitution value of 0.04 yields the brightest emission, here producing 1.3× the intensity of visible light emitted by the unmodified particles. Furthermore, UC intensity from the $x = 0.04$ nanoparticles was observed to surpass 10 000 counts per second at a 980 nm irradiance of 110 kW/cm$^2$. This is to our knowledge the highest single-particle NIR-to-visible UC emisssion intensity value reported for particles smaller than 50 nm, highlighting the merits of exploring cosubstitution for bioimaging purposes.

To definitively confirm that the radiative rate enhancement and subsequent UC quantum yield boost result from cosubstitution, we performed rigorous structural and compositional characterization of our samples. The host lattice structure of each $\beta$-NaY$_{0.8-2x}$Gd$_x$Lu$_x$F$_4$:Yb$_{0.18}$Er$_{0.02}$ sample was probed using XRD. Because it exclusively probes long-range, global order, XRD is the ideal method to confirm that the phase and the average unit cell are not affected by cosubstitution. Diffraction patterns for each sample are shown in Figure 4a. The chief quantities of interest are consistency in the number of peaks present and in the diffraction angles of the peaks.

Regarding the former, it is clear that no diffraction peaks emerge or disappear as the cosubstitution value is varied, demonstrating that no phase change is induced. Additionally, each of the peaks present can be indexed using the ICDD 016-0334 pattern (the standard for $\beta$-NaYF$_4$) with the exception of the peaks that occur at 36.9°, 38.0°, and 41°; these are aluminum peaks caused by diffraction from the sample holder (see SI). The peak positions remain constant throughout the series, suggesting the average unit cell remains unchanged as desired. In fact, the only noticeable (though slight) differences in the XRD patterns are in the breadths of the peaks. Particle size is largely responsible for this variation, although some broadening is also to be expected as $x$ is increased and the distribution in lattice spacings widens accordingly.

To more quantitatively assess the consistency in average unit cell size across the sample series, we extracted lattice parameter values by fitting each pattern using a Pawley routine[60] (see SI for additional details). The results are shown in Figure 4b,c. A slight increase as a function of cosubstitution value is apparent in both lattice constants $a$ and $c$. The total magnitude of this increase is 0.2% in both parameters. As discussed shortly, we believe this overall lattice size increase likely follows from incomplete Lu$^{3+}$ incorporation in the nanoparticles. As a result, the ratio of Gd$^{3+}$ to Lu$^{3+}$ present in the host matrices is slightly above unity, yielding a slight but steady lattice constant increase with cosusbstitution value. In conjunction with the phase purity highlighted by the XRD patterns, we are thus able to say with confidence that the only structural changes engendered by cosubstitution are limited as desired to the local scale.

Finally, we confirm experimentally that cosubstitution does not affect the efficiency with which Yb$^{3+}$ and Er$^{3+}$ are incorporated into the host lattice. The sensitivity of UC performance in lanthanide-based systems to the precise concentrations of lanthanide ions present has been thoroughly characterized;[31,43,48] thus, it is of paramount importance that the fractions of Yb$^{3+}$ and Er$^{3+}$ in our samples are not influenced by cosubstitution value. Figure 4d shows ion concentrations measured experimentally using ICP-OES (see SI for details). The experimental data are superimposed on lines that depict the target composition fractions. It is immediately apparent from the plot that the concentrations of both upconverting ions neither vary from sample to sample nor deviate significantly

from the target values of 0.18 for $Yb^{3+}$ and 0.02 for $Er^{3+}$. Regarding the composition of the host matrix, the measured fraction of $Lu^{3+}$ is consistently observed to be slightly below the target value. Conversely, both $Y^{3+}$ and $Gd^{3+}$ are correspondingly present in greater amounts than intended, suggesting these make up the balance of the lattice. We accordingly attribute the previously discussed increase in unit cell size to this $Lu^{3+}$-poor deviation from the target lattice composition. The salient point of Figure 4c, however, is that the consistency measured in the upconverting ion concentrations eliminates doping efficiency as a potentially spurious influence on UC quantum yield.

In summary, we have achieved a 1.6× enhancement in UC quantum yield by inducing local symmetry distortion in Yb,Er-doped nanoparticles. $Gd^{3+}$ and $Lu^{3+}$ are cosubstituted for $Y^{3+}$ to achieve local modification of the host matrix. We vary the cosubstitution value to determine the host composition that yields the most efficient UC. The NIR-to-visible UC quantum yield measured here of 0.074% is to our knowledge the highest value attained for sub-25 nm unshelled nanoparticles. We demonstrate that cosubstitution must be responsible for this enhancement by using TEM, XRD, and ICP-OES to confirm that the particle morphologies, phase and average unit cell, and composition fractions of $Yb^{3+}$ and $Er^{3+}$, respectively, are consistent throughout the sample series. Additionally, by measuring excited-state lifetimes and comparing them to the observed quantum yield data, we prove that cosubstituting $Gd^{3+}$ and $Lu^{3+}$ for $Y^{3+}$ does induce a radiative rate increase. Finally, we investigate single-particle emission intensity to evaluate these nanoparticles for bioimaging purposes and report a 1.3× volumetric emission enhancement as well as a record value for sub-50 nm particles of 10 000 counts per second under 110 $kW/cm^2$ of 980 nm light. Cosubstitution values beyond 0.04 are seen to yield diminished UC quantum yields as well as single-particle emission intensities, suggesting an increase in lattice defects with cosubstitution.

The approach demonstrated herein to enhance UC quantum yield is independent of particle size, suggesting that larger nanoparticles as well as bulk samples would exhibit a similar enhancement with cosubstitution. Furthermore, this technique focuses on manipulating the local environments of the active ions to make radiative emission more likely. It is thus to our knowledge the first to successfully and definitively mitigate the problematically low radiative rates endemic to lanthanide-based upconverting systems. Our work does not seek to address the significant problem of surface quenching in this materials system and others like it. Thus, combining our approach with the practice of adding an inert, passivating shell layer to the particles could engender even larger enhancements and is therefore the subject of ongoing research. Lastly, this work is not specific to Yb,Er-based UC systems. Rather, the insight gained here is broadly applicable and, when applied in tandem with other efficiency-boosting techniques, may lead to truly unprecedented UC quantum yield regimes.

## ASSOCIATED CONTENT

### $\mathbf{S}$ Supporting Information

The Supporting Information is available free of charge on the ACS Publications website at DOI: 10.1021/acsphotonics.6b00166.

Additional details regarding procedures followed and equipment used, ancillary data, and expanded discussion of results (PDF)

## AUTHOR INFORMATION

### Corresponding Authors
*E-mail: mwisser@stanford.edu.
*E-mail: asalleo@stanford.edu.
*E-mail: jdionne@stanford.edu.

### Notes
The authors declare no competing financial interest.

## REFERENCES

(1) Wang, F.; Deng, R.; Liu, X. Preparation of core-shell $NaGdF_4$ nanoparticles doped with luminescent lanthanide ions to be used as upconversion-based probes. Nat. Protoc. 2014, 9.163410.1038/nprot.2014.111

(2) Li, Z.; Zhang, Y. An efficient and user-friendly method for the synthesis of hexagonal-phase $NaYF_4$:Yb, Er/Tm nanocrystals with controllable shape and upconversion fluorescence. Nanotechnology 2008, 19, 345606.

(3) Li, Z.; Wang, Z.; Wang, L.; Qian, H. Facile synthesis and properties of spherical assemblies of $NaYF_4$ nanocrystals with consistent crystalline orientation. CrystEngComm 2011, 13, 7009.

(4) Li, Z.; Park, W.; Zorzetto, G.; Lemaire, J.-S.; Summers, C. J. Synthesis protocols for $\delta$-doped $NaYF_4$:Yb,Er. Chem. Mater. 2014, 26, 1770−1778.

(5) Lei, L.; Chen, D.; Huang, P.; Xu, J.; Zhang, R.; Wang, Y. Modifying the size and uniformity of upconversion Yb/Er: $NaGdF_4$ nanocrystals through alkaline-earth doping. Nanoscale 2013, 5, 11298−11305.

(6) Fischer, S.; Favilla, E.; Tonelli, M.; Goldschmidt, J. C. Record efficient upconverter solar cell devices with optimized bifacial silicon solar cells and monocrystalline $BaY_2F_8$:30% $Er^{3+}$ upconverter. Sol. Energy Mater. Sol. Cells 2015, 136, 127−134.

(7) Wang, F.; Liu, X. Recent advances in the chemistry of lanthanide-doped upconversion nanocrystals. Chem. Soc. Rev. 2009, 38, 976−989.

(8) Yu, H.; Cao, W.; Huang, Q.; Ma, E.; Zhang, X.; Yu, J. Upconversion performance improvement of $NaYF_4$:Yb, Er by Sn codoping: Enhanced emission intensity and reduced decay time. J. Solid State Chem. 2013, 207, 170−177.

(9) Wang, J.; Deng, R.; MacDonald, M. A.; Chen, B.; Yuan, J.; Wang, F.; Chi, D.; Hor, T. S. A.; Zhang, P.; Liu, G.; Han, Y.; Liu, X. Enhancing multiphoton upconversion through energy clustering at sublattice level. Nat. Mater. 2014, 13, 157−162.

(10) Park, Y. I.; Nam, S. H.; Kim, J. H.; Bae, Y. M.; Yoo, B.; Kim, H. M.; Jeon, K.-S.; Park, H. S.; Choi, J. S.; Lee, K. T.; Suh, Y. D.; Hyeon, T. Comparative study of upconverting nanoparticles with various crystal structures, core/shell structures, and surface characteristics. J. Phys. Chem. C 2013, 117, 2239−2244.

(11) Fischer, S.; Martín-Rodríguez, R.; Fröhlich, B.; Krämer, K. W.; Meijerink, A.; Goldschmidt, J. C. Upconversion quantum yield of $Er^{3+}$-doped $\beta$-$NaYF_4$ and $Gd_2O_2S$: The effects of host lattice, $Er^{3+}$ doping, and excitation spectrum bandwidth. *J. Lumin.* **2014**, *153*, 281−287.

(12) Xie, X.; Gao, N.; Deng, R.; Sun, Q.; Xu, Q.-H.; Liu, X. Mechanistic investigation of photon upconversion in $Nd^{3+}$-sensitized core-shell nanoparticles. *J. Am. Chem. Soc.* **2013**, *135*, 12608−12611.

(13) Wang, F.; Deng, R.; Wang, J.; Wang, Q.; Han, Y.; Zhu, H.; Chen, X.; Liu, X. Tuning upconversion through energy migration in core-shell nanoparticles. *Nat. Mater.* **2011**, *10*, 968−973.

(14) Wu, D. M.; García-Etxarri, A.; Salleo, A.; Dionne, J. A. Plasmon-enhanced upconversion. *J. Phys. Chem. Lett.* **2014**, *5*, 4020−4031.

(15) Saboktakin, M.; Ye, X.; Chettiar, U. K.; Engheta, N.; Murray, C. B.; Kagan, C. R. Plasmonic enhancement of nanophosphor upconversion luminescence in Au nanohole arrays. *ACS Nano* **2013**, *7*, 7186−7192.

(16) Zou, W.; Visser, C.; Maduro, J. A.; Pshenichnikov, M. S.; Hummelen, J. C. Broadband dye-sensitized upconversion of near-infrared light. *Nat. Photonics* **2012**, *6*, 560−564.

(17) Atre, A. C.; Dionne, J. A. Realistic upconverter-enhanced solar cells with non-ideal absorption and recombination efficiencies. *J. Appl. Phys.* **2011**, *110*, 034505.

(18) Boriskina, S.; et al. Roadmap on optical energy conversion. *J. Opt.* **2016**, *18*, 073004.

(19) Briggs, J. A.; Atre, A. C.; Dionne, J. A. Narrow-bandwidth solar upconversion: Case studies of existing systems and generalized fundamental limits. *J. Appl. Phys.* **2013**, *113*, 124509.

(20) Richards, B. S. Enhancing the performance of silicon solar cells via the application of passive luminescence conversion layers. *Sol. Energy Mater. Sol. Cells* **2006**, *90*, 2329−2337.

(21) Schulze, T. F.; Schmidt, T. W. Photochemical upconversion: present status and prospects for its application to solar energy conversion. *Energy Environ. Sci.* **2015**, *8*, 103.

(22) Shalav, A.; Richards, B. S.; Green, M. A. Luminescent layers for enhanced silicon solar cell performance: Up-conversion. *Sol. Energy Mater. Sol. Cells* **2007**, *91*, 829−842.

(23) Wang, H.-Q.; Batentschuk, M.; Osvet, A.; Pinna, L.; Brabec, C. J. Rare-earth ion doped up-conversion materials for photovoltaic applications. *Adv. Mater.* **2011**, *23*, 2675−2680.

(24) Strümpel, C.; McCann, M.; Beaucarne, G.; Arkhipov, V.; Slaoui, A.; Švrček, V.; del Cañizo, C.; Tobias, I. Modifying the solar spectrum to enhance silicon solar cell efficiency - An overview of available materials. *Sol. Energy Mater. Sol. Cells* **2007**, *91*, 238−249.

(25) Wang, H.-Q.; Stubhan, T.; Osvet, A.; Litzov, I.; Brabec, C. J. Up-conversion semiconducting $MoO_3$/Yb/Er nanocomposites as buffer layer in organic solar cells. *Sol. Energy Mater. Sol. Cells* **2012**, *105*, 196−201.

(26) Fischer, S.; Johnson, N. J. J.; Pichaandi, J.; Goldschmidt, J. C.; van Veggel, F. C. J. M. Upconverting core-shell nanocrystals with high quantum yield under low irradiance: On the role of isotropic and thick shells. *J. Appl. Phys.* **2015**, *118*, 193105.

(27) Goldschmidt, J. C.; Fischer, S. Upconversion for photovoltaics - a review of materials, devices, and concepts for performance enhancement. *Adv. Opt. Mater.* **2015**, *3*, 510−535.

(28) Liu, C.; Gao, Z.; Zeng, J.; Hou, Y.; Fang, F.; Li, Y.; Qiao, R.; Shen, L.; Lei, H.; Yang, W.; Gao, M. Magnetic/upconversion fluorescent $NaGdF_4$:Yb,Er nanoparticle-based dual-modal molecular probes for imaging tiny tumors in vivo. *ACS Nano* **2013**, *7*, 7227−7240.

(29) Carpenter, C. M.; Sun, C.; Pratx, G.; Liu, H.; Cheng, Z.; Xing, L. Radioluminescent nanophosphors enable multiplexed small-animal imaging. *Opt. Express* **2012**, *20*, 11598−11604.

(30) Chen, G.; Qiu, H.; Prasad, P. N.; Chen, X. Upconversion nanoparticles: design, nanochemistry, and applications in theranostics. *Chem. Rev.* **2014**, *114*, 5161−5214.

(31) Gargas, D. J.; Chan, E. M.; Ostrowski, A. D.; Aloni, S.; Altoe, M. V. P.; Barnard, E. S.; Sanii, B.; Urban, J. J.; Milliron, D. J.; Cohen, B. E.; Schuck, P. J. Engineering bright sub-10-nm upconverting nanocrystals for single-molecule imaging. *Nat. Nanotechnol.* **2014**, *9*, 300−305.

(32) Zhou, J.; Liu, Z.; Li, F. Upconversion nanophosphors for small-animal imaging. *Chem. Soc. Rev.* **2011**, *41*, 1323−1349.

(33) Xiong, L.; Chen, Z.; Tian, Q.; Cao, T.; Xu, C.; Li, F. High contrast upconversion luminescence target imaging in vivo using peptide-labeled nanophosphors. *Anal. Chem.* **2009**, *81*, 8687−8694.

(34) Naczynski, D. J.; Tan, M. C.; Zevon, M.; Wall, B.; Kohl, J.; Kulesa, A.; Chen, S.; Roth, C. M.; Riman, R. E.; Moghe, P. V. Rare-earth-doped biological composites as in vivo shortwave infrared reporters. *Nat. Commun.* **2013**, *4*, 2199.

(35) Liu, Q.; Yang, T.; Feng, W.; Li, F. Blue-emissive upconversion nanoparticles for low-power-excited bioimaging in vivo. *J. Am. Chem. Soc.* **2012**, *134*, 5390−5397.

(36) Liu, Q.; Sun, Y.; Yang, T.; Feng, W.; Li, C.; Li, F. Sub-10 nm hexagonal lanthanide-doped $NaLuF_4$ upconversion nanocrystals for sensitive bioimaging in vivo. *J. Am. Chem. Soc.* **2011**, *133*, 17122−17125.

(37) Zhou, B.; Shi, B.; Jin, D.; Liu, X. Controlling upconversion nanocrystals for emerging applications. *Nat. Nanotechnol.* **2015**, *10*, 924−936.

(38) Wu, S.; Butt, H.-J. Near-infrared-sensitive materials based on upconverting nanoparticles. *Adv. Mater.* **2016**, *28*, 1208−1226.

(39) Idris, N. M.; Gnanasammandhan, M. K.; Zhang, J.; Ho, P. C.; Mahendran, R.; Zhang, Y. In vivo photodynamic therapy using upconversion nanoparticles as remote-controlled nanotransducers. *Nat. Med.* **2012**, *18*, 1580−1585.

(40) Deng, R.; Qin, F.; Chen, R.; Huang, W.; Hong, M.; Liu, X. Temporal full-colour tuning through non-steady-state upconversion. *Nat. Nanotechnol.* **2015**, *10*, 237−242.

(41) Chen, Z.; He, S.; Butt, H.-J.; Wu, S. Photon upconversion lithography: Patterning of biomaterials using near-infrared light. *Adv. Mater.* **2015**, *27*, 2203−2206.

(42) Ai, X.; et al. In vivo covalent cross-linking of photon-converted rare-earth nanostructures for tumour localization and theranostics. *Nat. Commun.* **2016**, *7*, 10432.

(43) Boyer, J.-C.; van Veggel, F. C. J. M. Absolute quantum yield measurements of colloidal $NaYF_4$: $Er^{3+}$, $Yb^{3+}$ upconverting nano-particles. *Nanoscale* **2010**, *2*, 1417−1419.

(44) Wang, F.; Wang, J.; Liu, X. Direct evidence of a surface quenching effect on size-dependent luminescence of upconversion nanoparticles. *Angew. Chem.* **2010**, *122*, 7618−7622.

(45) Dodson, C. M.; Zia, R. Magnetic dipole and electric quadrupole transitions in the trivalent lanthanide series: Calculated emission rates and oscillator strengths. *Phys. Rev. B: Condens. Matter Mater. Phys.* **2012**, *86*, 125102.

(46) Renero-Lecuna, C.; Martín-Rodríguez, R.; Valiente, R.; González, J.; Rodríguez, F.; Krämer, K. W.; Güdel, H. U. Origin of the high upconversion green luminescence efficiency in $\beta$-$NaYF_4$:2% $Er^{3+}$,20%$Yb^{3+}$. *Chem. Mater.* **2011**, *23*, 3442−3448.

(47) Wisser, M. D.; Chea, M.; Lin, Y.; Wu, D. M.; Mao, W. L.; Salleo, A.; Dionne, J. A. Strain-induced modification of optical selection rules in lanthanide-based upconverting nanoparticles. *Nano Lett.* **2015**, *15*, 1891−1897.

(48) Chan, E. M.; Gargas, D. J.; Schuck, P. J.; Milliron, D. J. Concentrating and recycling energy in lanthanide codopants for efficient and spectrally pure emission: The case of $NaYF_4$:$Er^{3+}$/$Tm^{3+}$ upconverting nanocrystals. *J. Phys. Chem. B* **2012**, *116*, 10561−10570.

(49) Laporte, O.; Meggers, W. F. Some rules of spectral structure. *J. Opt. Soc. Am.* **1925**, *11*, 459−463.

(50) Shannon, R. D. Revised effective ionic radii and systematic studies of interatomic distances in halides and chalcogenides. *Acta Crystallogr., Sect. A: Cryst. Phys., Diffr., Theor. Gen. Crystallogr.* **1976**, *32*, 751.

(51) Aebischer, A.; Hostettler, M.; Hauser, J.; Krämer, K.; Weber, T.; Güdel, H. U.; Bürgi, H.-B. Structural and spectroscopic character-ization of active sites in a family of light-emitting sodium lanthanide tetrafluorides. *Angew. Chem., Int. Ed.* **2006**, *45*, 2802−2806.

(52) Cheng, Q.; Sui, J.; Cai, W. Enhanced upconversion emission in $Yb^{3+}$ and $Er^{3+}$ codoped $NaGdF_4$ nanocrystals by introducing $Li^+$ ions. *Nanoscale* **2012**, *4*, 779−784.

(53) Tian, G.; Gu, Z.; Zhou, L.; Yin, W.; Liu, X.; Yan, L.; Jin, S.; Ren, W.; Xing, G.; Li, S.; Zhao, Y. $Mn^{2+}$ dopant-controlled synthesis of $NaYF_4$:Yb/Er upconversion nanoparticles for in vivo imaging and drug delivery. *Adv. Mater.* **2012**, *24*, 1226−1231.

(54) Guo, L.; Wang, Y.; Wang, Y.; Zhang, J.; Dong, P.; Zeng, W. Structure, enhancement and white luminescence of multifunctional $Lu_6O_5F_8$:20%$Yb^{3+}$,1%$Er^{3+}$($Tm^{3+}$) nanoparticles via further doping with $Li^+$ under different excitation sources. *Nanoscale* **2013**, *5*, 2491−2504.

(55) Mahalingam, V.; Naccache, R.; Vetrone, F.; Capobianco, J. A. Enhancing upconverted white light in $Tm^{3+}$/ $Yb^{3+}$/ $Ho^{3+}$-doped $GdVO_4$ nanocrystals via incorporation of $Li^+$ ions. *Opt. Express* **2012**, *20*, 111−119.

(56) Yin, W.; Zhao, L.; Zhou, L.; Gu, Z.; Liu, X.; Tian, G.; Jin, S.; Yan, L.; Ren, W.; Xing, G.; Zhao, Y. Enhanced red emission from $GdF_3$:$Yb^{3+}$,$Er^{3+}$ upconversion nanocrystals by $Li^+$ doping and their application for bioimaging. *Chem. - Eur. J.* **2012**, *18*, 9239−9245.

(57) Yuan, D.; Tan, M. C.; Riman, R. E.; Chow, G. M. Comprehensive study on the size effects of the optical properties of $NaYF_4$:Yb,Er nanocrystals. *J. Phys. Chem. C* **2013**, *117*, 13297−13304.

(58) Berry, M. T.; May, P. S. Disputed mechanism for NIR-to-red upconversion luminescence in $NaYF_4$:$Yb^{3+}$,$Er^{3+}$. *J. Phys. Chem. A* **2015**, *119*, 9805−9811.

(59) Dieke, G. H.; Crosswhite, H. M. The spectra of the doubly and triply ionized rare earths. *Appl. Opt.* **1963**, *2*, 675−686.

(60) Pawley, G. S. Unit-cell refinement from powder diffraction scans. *J. Appl. Crystallogr.* **1981**, *14*, 357−361.